



A Series of BRAF- and NRAS-Driven Murine Melanoma Cell Lines with Inducible Gene Modulation Capabilities

Ilah Bok^{1,2}, Ariana Angarita¹, Stephen M. Douglass³, Ashani T. Weeraratna^{3,4} and Florian A. Karreth¹

Murine cancer cell lines are powerful research tools to complement studies in genetically engineered mouse models. We have established 21 melanoma cell lines from embryonic stem cell-genetically engineered mouse models driven by alleles that model the most frequent genetic alterations in human melanoma. In addition, these cell lines harbor regulatory alleles for the genomic integration of transgenes and the regulation of expression of such transgenes. In this study, we report a comprehensive characterization of these cell lines. Specifically, we validated melanocytic origin, driver allele recombination and expression, and activation of the oncogenic MAPK and protein kinase B pathways. We further tested tumor formation in syngeneic immunocompetent recipients as well as the functionality of the integrated Tet-ON system and recombination-mediated cassette exchange homing cassette. Finally, by deleting the transcription factor MAFG with an inducible CRISPR/Cas9 approach, we show the utility of the regulatory alleles for candidate gene modulation. These cell lines will be a valuable resource for studying melanoma biology and therapy.

JID Innovations (2022);2:100076 doi:10.1016/j.xjidi.2021.100076

INTRODUCTION

Genetically engineered mouse models (GEMMs) have significantly advanced our understanding of the pathobiology of melanoma; however, the use of GEMMs is expensive and cumbersome. The generation of GEMM-derived melanoma cell lines (Hooijkaas et al., 2012; Jenkins et al., 2014; Koya et al., 2012; Meeth et al., 2016; Pérez-Guijarro et al., 2020; Wang et al., 2017), especially those that can be allografted into syngeneic immunocompetent recipients, has alleviated some of the shortcomings of GEMMs. Indeed, the Yale University Mouse Melanoma series (Meeth et al., 2016) as well as the UV-irradiated derivative YUMMER1.7 (Wang et al., 2017) are widely used tools in basic and preclinical melanoma research. Most cell lines were derived from melanoma GEMMs where *Braf*^{V600E} is expressed from its

endogenous locus. Only a few *Nras*-mutant cell lines have been established, all of which were derived from models where a transgenic *Nras* oncogene is under the control of the tyrosinase promoter (*Tyr::Nras*^{Q61K}) (Dorard et al., 2017; Lindsay et al., 2011; Petit et al., 2019; Swoboda et al., 2021). Murine cell lines derived from melanomas driven by the endogenous *LSL-Nras*^{Q61R} allele (Burd et al., 2014) have not been reported. Moreover, the field would benefit from murine melanoma cell lines harboring alleles that enable the efficient modulation of genes of interest.

We recently established a speedy mouse modeling platform that relies on efficient targeting of multiallelic embryonic stem cells (ESCs) to produce chimeras as experimental animals (Bok et al., 2020). These newly derived ESCs contain driver alleles that model the most common genetic alterations in human melanoma (*Braf*^{V600E}, *Nras*^{Q61R}, *Pten*^{Δ/Δ}, *Cdkn2a*^{Δ/Δ}). Moreover, the ESCs contain alleles enabling the integration of transgenes through recombination-mediated cassette exchange (RMCE) and the regulation of such transgenes through the Tet-ON system. We previously derived 17 cell lines from melanomas that arose in chimeras generated from untargeted ESCs (Bok et al., 2020). In this study, we report the establishment of another 4 murine melanoma cell lines and the systematic characterization of key features for the 21 cell lines. Furthermore, by inducible CRISPR/Cas9-mediated depletion of MAFG, a transcription factor we recently identified as a potential vulnerability of melanoma (Vera et al., 2021), we show the utility of the integrated regulatory elements for the characterization of genes of interest.

RESULTS AND DISCUSSION

We previously reported the derivation of 17 melanoma cell lines (Table 1) from ESC-derived GEMMs chimeras (Bok et al., 2020). These lines harbor allele combinations that model the

¹Department of Molecular Oncology, H. Lee Moffitt Cancer Center and Research Institute, Tampa, Florida, USA; ²Cancer Biology PhD program, Department of Cell Biology, Microbiology and Molecular Biology, College of Arts and Sciences, University of South Florida, Tampa, Florida, USA; ³Department of Biochemistry and Molecular Biology, Johns Hopkins Bloomberg School of Public Health, Johns Hopkins University, Baltimore, Maryland, USA; and ⁴Department of Oncology, The Sidney Kimmel Comprehensive Cancer Center, Johns Hopkins School of Medicine, University, Baltimore, Maryland, USA

Correspondence: Florian A. Karreth, Department of Molecular Oncology, H. Lee Moffitt Cancer Center and Research Institute, 12902 Magnolia Drive, Tampa, Florida 33612-9416, USA. E-mail: florian.karreth@moffitt.org

Abbreviations: BCC, *Braf*^{V600E}; *Cdkn2a*^{Δ/Δ}; BPP, *Braf*^{V600E}; *Pten*^{Δ/Δ}; CHC, collagen homing cassette; Dox, doxycycline; ESC, embryonic stem cell; FBS, fetal bovine serum; GEMM, genetically engineered mouse model; NCC, *Nras*^{Q61R}; *Cdkn2a*^{Δ/Δ}; NPP, *Nras*^{Q61R}; *Pten*^{Δ/Δ}; RMCE, recombination-mediated cassette exchange; sgRNA, single-guide RNA

Received 6 May 2021; revised 30 September 2021; accepted 2 November 2021; accepted manuscript published online XXX; corrected proof published online XXX

Cite this article as: *JID Innovations* 2022;2:100076

Table 1. Overview of the 21 Established Murine Melanoma Cell Lines

Genotype	Cell Lines	Grows in BL/6	rtTA3 Expression	CHC Targeting	Source
BPP	M10M1	Yes	Yes	No	Bok et al., 2020
BPP	M10M2	Yes	No	No	Bok et al., 2020
BPP	M10M3	Yes	Yes	No	Bok et al., 2020
BPP	M10M4	No	Yes	No	Bok et al., 2020
BPP	M10M5	Yes	No	No	Bok et al., 2020
BPP	M10M6	Yes	Yes	No	Bok et al., 2020
BPP	M10M7	Yes	No	Yes	Bok et al., 2020
BPP	M27M1	Yes	No	Yes	Bok et al., 2020
BPP	M36M1	Yes	No	Yes	Bok et al., 2020
BPP	M36M2	Yes	No	No	Bok et al., 2020
BPP	M36M3	No	No	No	Bok et al., 2020
BCC	M161M1	Yes	No	Yes	Bok et al., 2020
BCC	M161M2	No	Yes	No	Bok et al., 2020
BCC	M167M1	Yes	No	Yes	Bok et al., 2020
NPP	M171M1	Yes	No	No	Bok et al., 2020
NPP	M173M1	Yes	No	No	Bok et al., 2020
NPP	M173M2	Yes	No	No	This paper
NPP	M175M1	No	Yes	Yes	Bok et al., 2020
NPP	M175M2	Yes	Yes	Yes	This paper
NCC	M133M1	No	No	No	This paper
NCC	M133M2	Yes	Yes	No	This paper

Abbreviations: BCC, *Braf*^{V600E}, *Cdkn2a*^{Δ/Δ}; BPP, *Braf*^{V600E}, *Pten*^{Δ/Δ}; CHC, collagen-homing cassette; NCC, *Nras*^{Q61R}, *Cdkn2a*^{Δ/Δ}; NPP, *Nras*^{Q61R}, *Pten*^{Δ/Δ}. The cell lines were derived from mice from four different backgrounds: BPP (LSL-*Braf*^{V600E}, *Pten*^{FL/FL}; Tyr-CreERT2; CAGs-LSL-rtTA3, CHC), NPP (LSL-*Nras*^{Q61R}, *Pten*^{FL/FL}; Tyr-CreERT2; CAGs-LSL-rtTA3, CHC), BCC (LSL-*Braf*^{V600E}, *Cdkn2a*^{FL/FL}; Tyr-CreERT2; CAGs-LSL-rtTA3, CHC), and NCC (LSL-*Nras*^{Q61R}, *Cdkn2a*^{FL/FL}; Tyr-CreERT2; CAGs-LSL-rtTA3, CHC). The ability of the cell lines to form tumors when transplanted into syngeneic C57BL/6 recipients, the expression of the reverse tetracycline-transactivator, and the capability of targeting the collagen-homing cassette through recombination-mediated cassette exchange are indicated. Source indicates whether the cell lines were previously derived (Bok et al., 2020) or established as part of this study.

most frequent genetic alterations in human melanoma (*Braf*^{V600E}, *Nras*^{Q61R}, *Pten*^{Δ/Δ}, *Cdkn2a*^{Δ/Δ}), the Tyr-CreERT2 and CAGs-LSL-rtTA3 regulatory alleles, and the collagen homing cassette (CHC) for RMCE (Bok et al., 2020). We established four additional mouse melanoma cell lines (Table 1) for a total of 11 *Braf*^{V600E}, *Pten*^{Δ/Δ} (BPP) lines, 5 *Nras*^{Q61R}, *Pten*^{Δ/Δ} (NPP) lines, 3 *Braf*^{V600E}, *Cdkn2a*^{Δ/Δ} (BCC) lines, and 2 *Nras*^{Q61R}, *Cdkn2a*^{Δ/Δ} (NCC) lines (Table 1). All BCC and NCC melanoma lines could be readily established. Conversely, BPP and NPP cells quickly entered growth arrest in vitro. We therefore transplanted BPP and NPP cells into immunocompromised Nu/Nu mice before entering growth arrest, allowed for tumors to grow, and derived cell lines from these tumors.

We first validated the melanocytic origin of the cell lines. All lines expressed the melanoma markers S100B and/or MART1 (Figure 1a). Interestingly, *Mitf* expression is significantly downregulated in ESC-derived GEMM melanomas and all cell lines derived from them (Figure 2a and b). Accordingly, expression of other melanocytic markers such as *Tyr*, *Tyrb2*, or *Silver* was abrogated in ESC-derived GEMM melanomas (Figure 2c), and we therefore did not examine their expression in the cell lines. We further performed genotyping PCRs on genomic DNA isolated from the cell lines to test the recombination of the LSL cassettes in the LSL-*Braf*^{V600E} and LSL-*Nras*^{Q61R} alleles. The LSL cassettes were removed in all cell lines (Figure 1b and c), and given that the Tyr-CreERT2 allele is only expressed in cells of the melanocytic lineage, this further suggests that our cell lines are indeed derived from melanomas. The wild-type *Nras* allele was lost in two

NPP (M173M2 and M173M2) and one NCC (M133M1) cell line (Figure 1c), which was confirmed by Sanger sequencing (data not shown). Interestingly, loss of heterozygosity in *Nras* mutant human melanoma cell lines has been reported previously (Jeck et al., 2014), indicating that the wild-type *Nras* allele may also oppose the oncogenic effects of mutant *Nras* in murine melanomas. Curiously, two NPP cell lines (M175M1 and M175M2) underwent an aberrant recombination reaction where the three SV40 polyadenylation signals and the 3' loxP site were excised, but the 5' loxP site was retained, resulting in a larger recombined LSL band in the genotyping PCR reaction (Figure 1c). However, these two cell lines express mutant *Nras*^{Q61R}, as confirmed by Sanger sequencing of exon 2 (Figure 1d). The M175M1 and M175M2 cell lines were derived from two different tumors from the same mouse. We validated the lack of the aberrant recombination in the ESC line used to generate this NPP chimera (data not shown), indicating that the recombination occurred in the mouse. It seems unlikely, albeit possible, that the aberrant recombination occurred in parallel in two melanocytes that then gave rise to two independent tumors. Rather, the aberrant recombination may have occurred during development in a common melanocyte precursor, or one tumor is a skin metastasis of the other. Either way, because the LSL was partially removed, and mutant *Nras*^{Q61R} is expressed, the M175M1 and M175M2 cell lines are equivalent to the other NPP cell lines that underwent the canonical LSL excision.

The requirement for BPP and NPP cell lines to undergo an in vivo passage indicates that additional genetic changes

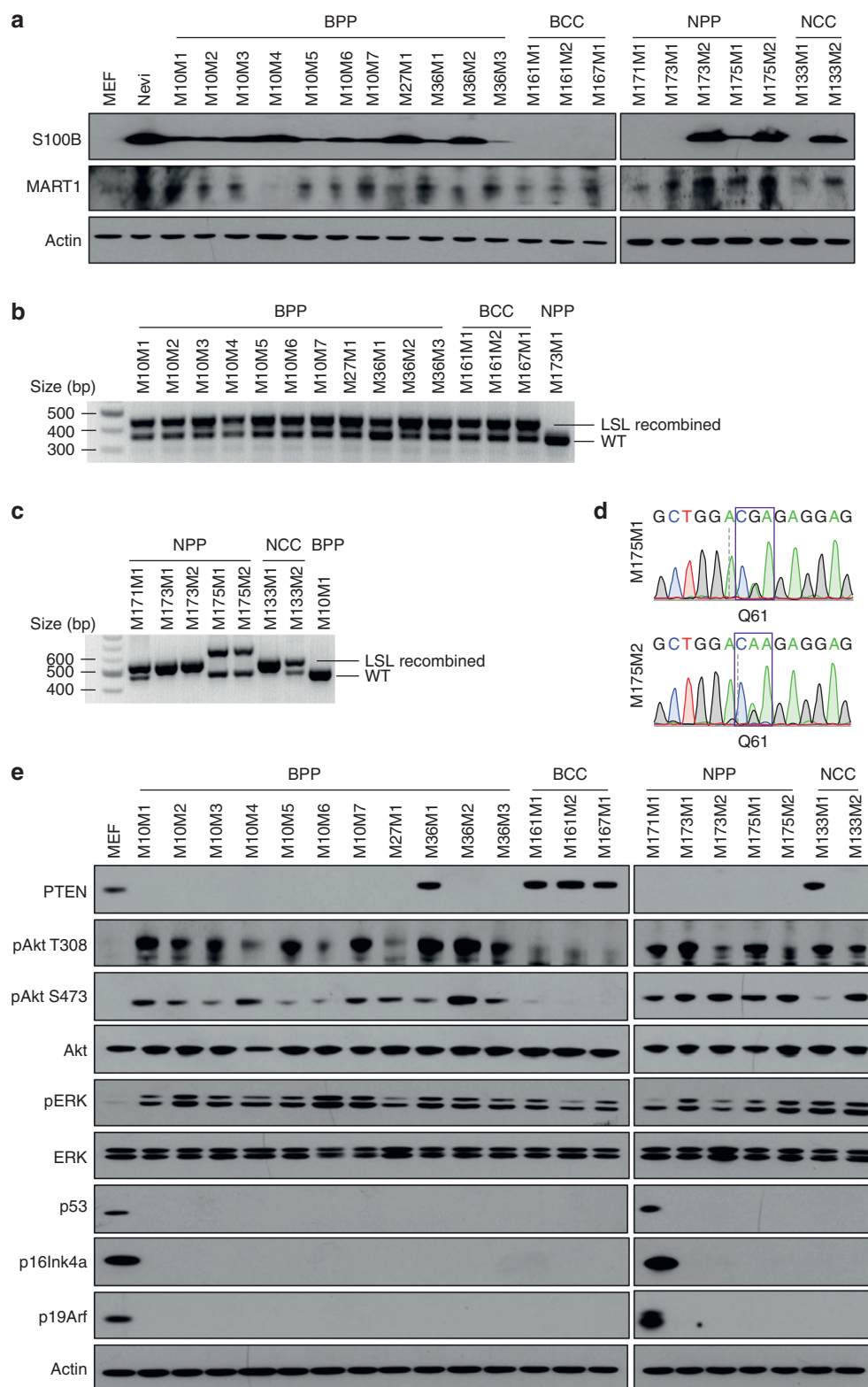


Figure 1. Validation of mouse melanoma cell line lineage, tumor suppressor expression, and Akt and ERK signaling. (a) Melanoma markers S100B and MART1 expression was assessed in the 21 murine melanoma cell lines by western blot. MEFs and nevi collected from hyperpigmented mouse skin were included as negative control and positive controls, respectively. (b) Analysis of LSL recombination of the LSL-*Brat*^{V600E} allele by genotyping PCR. (c) Analysis of LSL recombination of the LSL-*Nras*^{Q61R} allele by genotyping PCR. (d) M175M1 and M175M2 cell lines express both the WT (CAA) and mutant (CGA) *Nras*^{Q61} alleles. (e) PTEN, p16Ink4a, p19Arf, and p53 expression in the 21 murine melanoma cell lines was assessed by western blot. All but one *Pten*^{Δ/Δ}-derived cell line lost *Pten* expression. *Cdkn2a*^{Δ/Δ}-derived cell lines maintained PTEN expression except for one NCC cell line. BPP and NPP cells lost p16Ink4a, p19Arf, and p53 expression except for one NPP line. MEFs were used as a positive control. MAPK and Akt pathway activation was also evaluated. BPP, NPP, and the PTEN-deficient NCC cell lines showed elevated pAkt. All cell lines exhibited elevated pErk expression. Akt, protein kinase B; BCC, *Brat*^{V600E}; *Cdkn2a*^{Δ/Δ}; BPP, *Brat*^{V600E}; *Pten*^{Δ/Δ}; bp, base pair; ERK, extracellular signal–regulated kinase; MEF, mouse embryonic fibroblast; NPP, *Nras*^{Q61R}; *Pten*^{Δ/Δ}; pAkt, phosphorylated protein kinase B; pERK, phosphorylated extracellular signal–regulated kinase; WT, wild type.

need to occur to enable the establishment of cell lines, most likely alterations in the *Cdkn2a* and or *p53* genes. We therefore assessed the expression levels of p16Ink4a, p19Arf, and p53. Interestingly, except for one cell line, p16Ink4a, p19Arf, and p53 expression was undetectable in BPP and NPP cell lines (Figure 1e). As expected, BCC and NCC cell

lines do not express p16Ink4a, p19Arf, or p53 (Figure 1e). We also analyzed the expression of PTEN and found that it was retained in one BPP cell line, whereas PTEN was undetectable in all the other BPP and NPP cell lines (Figure 1e). All BCC cell lines retained PTEN expression as did one NCC cell line, whereas the second NCC cell line surprisingly lost PTEN

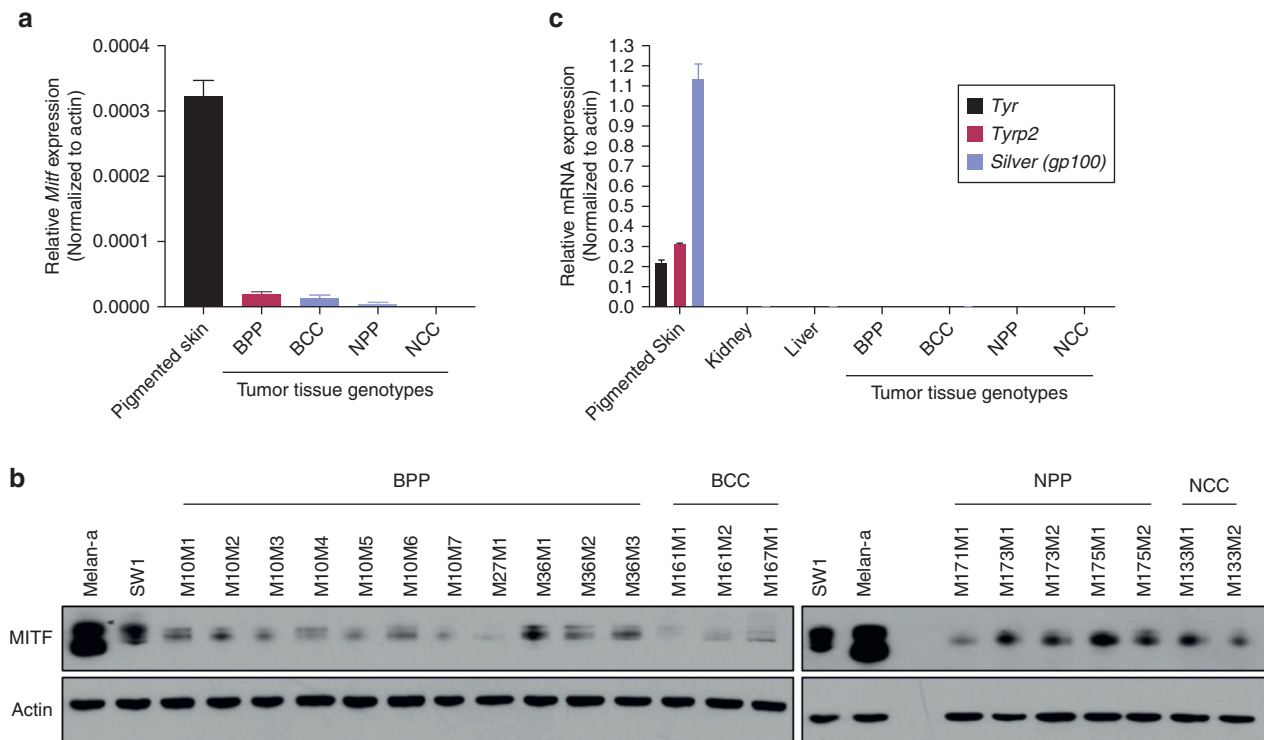


Figure 2. Expression of melanoma markers in ESC-derived GEMM melanomas. (a) Pigmented skin or melanomas from BPP, BCC, NPP, and NCC chimeras were collected, and *Mitf* mRNA expression was measured by RT-qPCR. *Mitf* expression was significantly reduced in melanoma compared to pigmented skin. (b) MITF protein expression in murine melanoma cell lines was analyzed by western blot. Mouse melanocyte cell line melan-a and melanoma cell line SW1 were used as MITF-positive controls. (c) *Tyr*, *Tyrp2*, and *Silver (gp100)* mRNA expression was measured in pigmented skin, normal kidney and liver tissues, and melanomas from BPP, BCC, NPP, NCC chimeras. Melanomas from chimeras do not express *Tyr*, *Tyrp2*, and *Silver*. BCC, *Braf*^{V600E}; *Cdkn2a*^{Δ/Δ}; BPP, *Braf*^{V600E}; *Pten*^{Δ/Δ}; ESC, embryonic stem cell; GEMM, genetically engineered mouse model; NCC, *Nras*^{Q61R}; *Cdkn2a*^{Δ/Δ}; NPP, *Nras*^{Q61R}; *Pten*^{Δ/Δ}.

expression (Figure 1e). We next tested the activation of oncogenic pathways in the melanoma cell lines and found that, as expected, BPP and NPP cell lines displayed increased protein kinase B activation compared with BCC and NCC lines (Figure 1e). Extracellular signal-regulated kinase activation was increased compared with that in mouse embryonic fibroblasts, varied between cell lines, and was not associated with a particular genotype (Figure 1e). Thus, our cell lines are of melanocytic origin, have recombined the relevant alleles, and exhibit activation of the appropriate oncogenic pathways. Moreover, BPP and NPP cell lines inactivated p16Ink4a, p19Arf, and p53 expression.

We next explored the utility of the regulatory alleles, Tyr-CreERT2, CAGS-LSL-rTA3, and CHC. Cre expression was lost in all the 21 cell lines (Bok et al., 2020 and Figure 3a), and given that tyrosinase is undetectable in ESC-derived GEMM melanomas (Figure 2c), this indicates that Tyr-CreERT2 expression is attenuated as well. To test whether the rTA3 transactivator is active, we transduced all cell lines with a doxycycline (Dox)-inducible lentiviral TRE-GFP construct. Adding Dox to the culture media and analyzing GFP expression revealed rTA3 activity in eight cell lines (Table 1). Lack of rTA3 activity in the remaining cell lines is likely due to failed recombination of the CAGS-LSL-rTA3 allele. Accordingly, rTA3 activity was readily induced by delivery of adenoviral Cre recombinase to a TRE-GFP-transduced BPP cell line as measured by GFP positivity (Figure 3b). Furthermore, using a constitutively active EF1α-

GFP construct, we found that seven lines are amenable to CHC targeting by RMCE (Table 1). We surmise that optimizing the transfection and selection conditions will enable successful CHC targeting in the remaining lines. Thus, although Tyr-CreERT2 is inactivated in all the cell lines, rTA3 is active in eight cell lines and can likely be activated in the remaining lines. We found CHC targeting by RMCE to be possible in several lines and further optimization could improve the targeting success rate.

The ESCs used to generate chimeras and thus the melanomas from which we derived the cell lines are on an almost pure C57BL/6 background. To determine the suitability of the murine cell lines for syngeneic allografts, we subcutaneously transplanted 1×10^6 cells of each line into C57BL/6 recipient mice and found that 16 cell lines formed tumors (Table 1). Three of the five cell lines (M10M4, M36M3, and M175M1) did not form tumors in C57BL/6 recipients despite forming tumors in Nu/Nu mice when we established them. This suggests that antitumor immunity prevents the growth of these cell lines in C57BL/6 mice. The remaining two cell lines, M161M2 and M133M1, have not been transplanted into Nu/Nu or C57BL/6 recipients, and their ability to form tumors in immunocompromised hosts is currently unknown. To further analyze potential antitumor immunity, we injected 0.25×10^6 cells of a BCC line (M167M1) into C57BL/6 recipients. This resulted in initial tumor growth, followed by transient tumor regression (Figure 4a), suggesting some antitumor immunity. Interestingly, antitumor immunity was

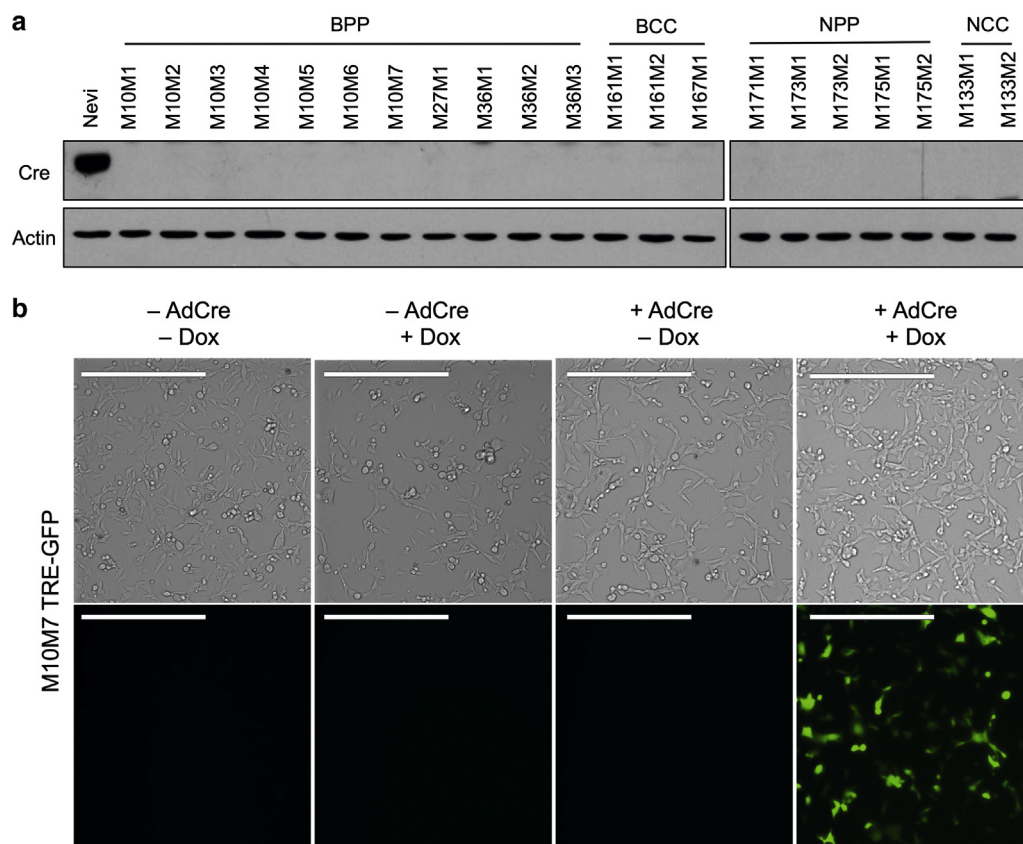


Figure 3. Loss of Cre expression and rTA3 activation by exogenous Cre.

(a) Cre expression was tested by western blot and found to be absent in the 21 cell lines. Nevi isolated from hyperpigmented mouse skin of a BPP chimera was used as a positive control. (b) Parental M10M7 cells showed no rTA3 activity likely owing to failed excision of the LSL cassette in the CAGS-LSL-rTA3 allele. M10M7 cells were infected with lentivirus carrying TRE-GFP, followed by AdCre recombinase. On Dox treatment, cells infected with AdCre expressed GFP, indicating successful LSL removal and rTA3 expression. Bar = 2 mm. AdCre, adenoviral Cre; BCC, *Braf*^{V600E}, *Cdkn2a*^{ΔΔ}; BPP, *Braf*^{V600E}, *Pten*^{ΔΔ}, Dox, doxycycline; NCC, *Nras*^{Q61R}, *Cdkn2a*^{ΔΔ}; NPP, *Nras*^{Q61R}, *Pten*^{ΔΔ}.

boosted when M167M1 tumor-bearing C57BL/6 recipients were treated with anti-PD-1 checkpoint inhibitor (Figure 4b). Another BCC cell line, M161M1, did not respond to anti-PD-1 treatment (Figure 4c), indicating that sensitivity to checkpoint inhibition is not a universal feature of our murine melanoma cell lines.

We next assessed how the regulatory alleles, specifically the rTA3 transactivator, can be employed for inducible gene modulation in the murine melanoma cell lines. To this end, we delivered Dox-inducible lentiviral TRE-Cas9 and tested the effect of continuous Cas9 expression on tumor growth.

Although Dox treatment had no effect on parental M167M1 cells (Figure 5a and b), Dox moderately slowed tumor growth of cells stably transduced with Dox-inducible TRE-Cas9. This occurred in immunocompromised NSG mice and syngeneic C57BL/6 mice (Figure 5c and d), indicating that in this context, Cas9 does not elicit an immune response but rather cell-intrinsically affects growth. A similar effect was observed for M10M3 cells when transplanted into NSG mice (Figure 5e and f). Thus, transient expression of Cas9 may be desirable. We confirmed that Dox withdrawal quickly turned off Cas9 expression in four cell lines (Figure 5g). To test the efficiency

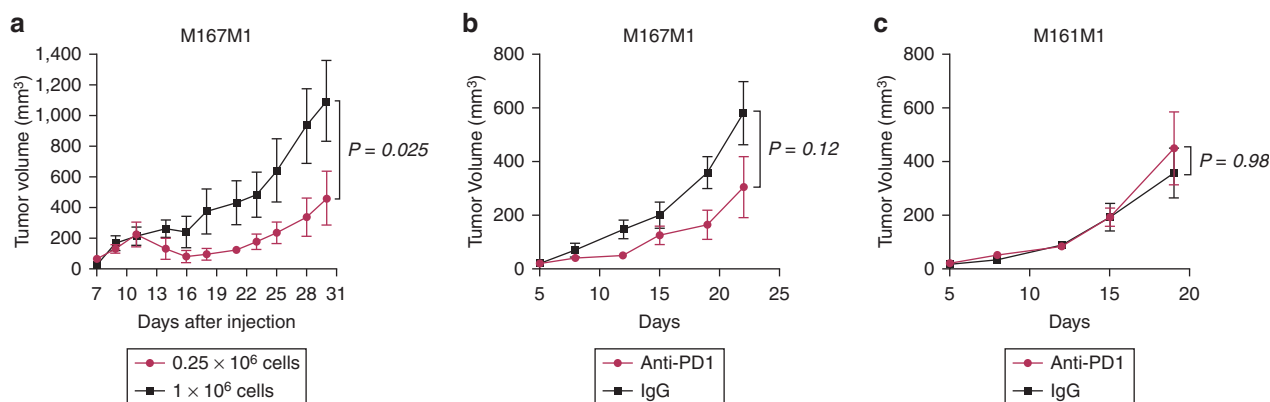


Figure 4. Melanoma growth in C57BL/6 mice and response to anti-PD-1 checkpoint inhibitor. (a) Different numbers of M167M1 (BCC) cells were injected into C57BL/6 mice. Whereas injecting 1×10^6 cells led to continuous tumor growth, injecting only 0.25×10^6 cells resulted in initial growth, followed by transient regression on day 14 and recovery after approximately 1 week. (b, c) M167M1 or M161M1 (BCC) cells were injected into C57BL/6 mice and treated with anti-PD-1 or IgG. Anti-PD-1 slowed tumor growth of the M167M1 model but had no effect on M161M1 tumor growth. BCC, *Braf*^{V600E}; *Cdkn2a*^{ΔΔ}.

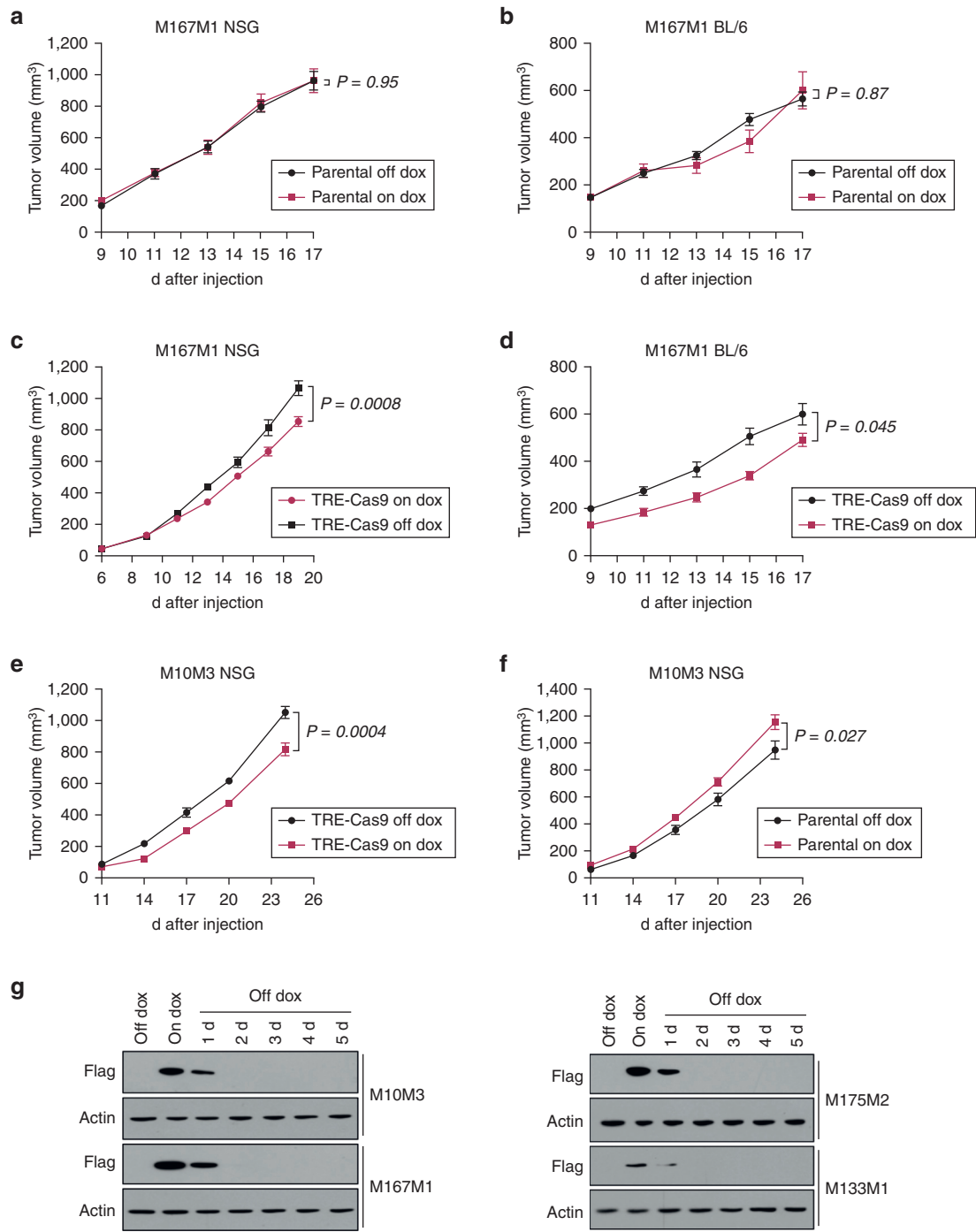


Figure 5. Utility of inducible Cas9 in murine melanoma cell lines. (a, b) M167M1 (BCC) parental cells were injected into NSG or C57BL/6 mice, which were fed 200 mg/kg Dox chow or a regular diet. Tumor volume was measured every 2 d. There was no effect on tumor growth when mice were fed Dox chow. (c, d) M167M1 (BCC) cells transduced with TRE-Cas9 were injected into NSG or C57BL/6 mice. Expression of Cas9 moderately reduced tumor growth in both NSG and C57BL/6 mice. (e) M10M3 (BPP) cells transduced with TRE-Cas9 were injected into NSG mice. Mice on Dox diet exhibited a moderate decrease in tumor growth. (f) M10M3 parental cells were injected into NSG mice. The Dox diet had no negative effect on tumors and even slightly increased tumor growth compared with tumors in the regular diet group. (g) M10M3 (BPP), M167M1 (BCC), M175M2 (NPP), and M133M1 (BCC) cell lines harboring TRE-Cas9 were treated with Dox for 2 d, followed by Dox removal for 5 d. Flag-tagged Cas9 expression was analyzed by western blot and was found to cease rapidly. BCC, *Braf*^{V600E}; Cdkn2a^{Δ/Δ}; BPP, *Braf*^{V600E}; *Pten*^{Δ/Δ}; d, day; Dox, doxycycline; NPP, *Nras*^{Q61R}; *Pten*^{Δ/Δ}.

of inducible TRE-Cas9, we delivered a CRISPR/Cas9 reporter consisting of a GFP cDNA and a GFP-targeting sgRNA (Figure 6a). On Dox treatment, GFP expression was reduced (Figure 6b), thus validating Cas9 activity. To demonstrate the utility of Dox-inducible TRE-Cas9, we delivered a sgRNA

targeting *Mafig* to two murine melanoma lines, a transcription factor we recently found to be important for the proliferation of melanoma cells (Vera et al., 2021) (Figure 6a). Dox treatment reduced *Mafig* expression in TRE-Cas9 melanoma lines harboring a *Mafig*-targeting sgRNA (Figure 6c). Interestingly,

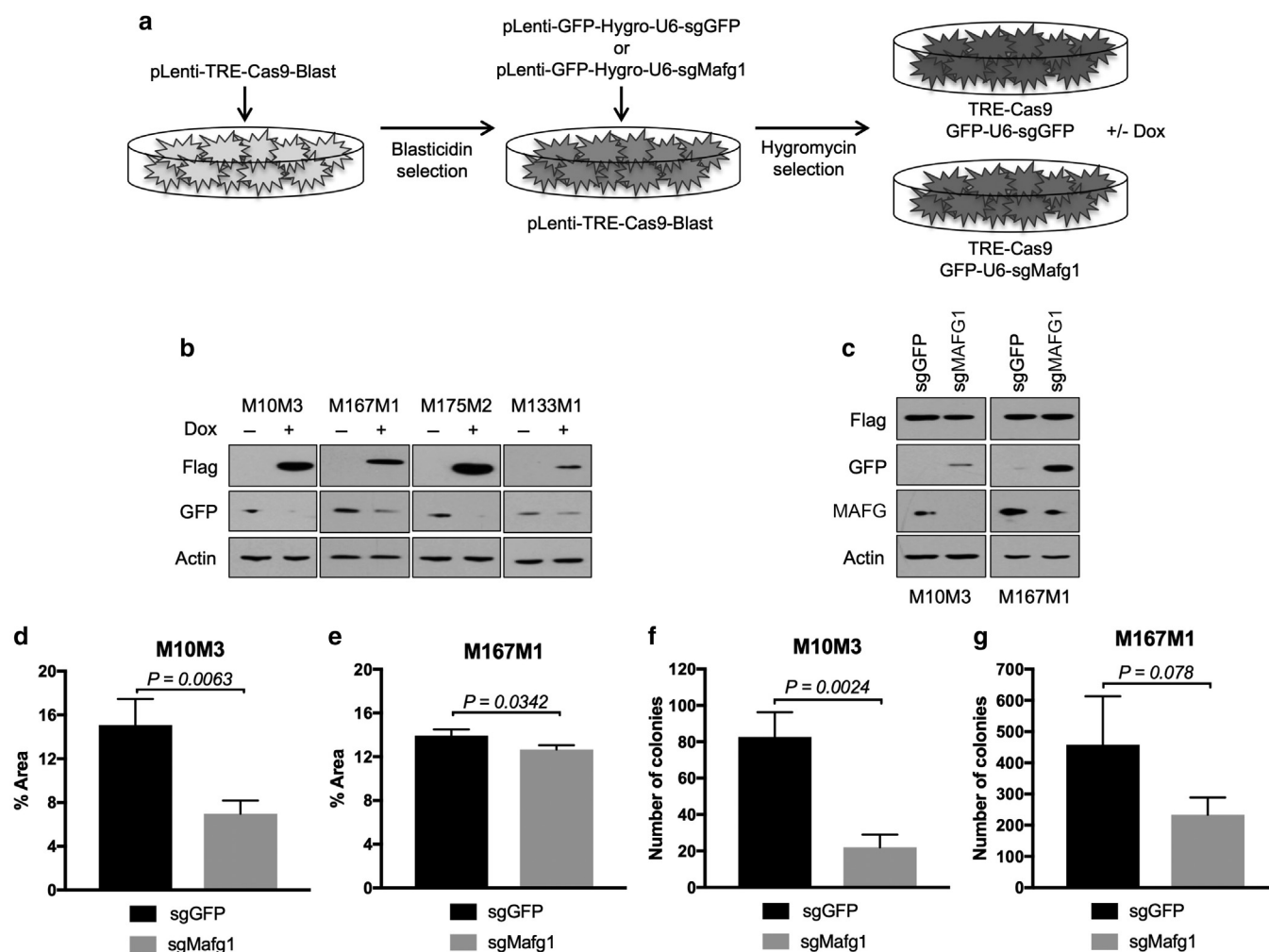


Figure 6. Inducible gene modulation in murine melanoma cell lines. (a) Schematic depicting the generation of stable cell lines expressing inducible Cas9 and sgRNA targeting GFP or *Mafg*. Mouse melanoma cell lines were infected with a lentiviral construct expressing Dox-inducible Cas9 and selected with blasticidin. Subsequently, TRE-Cas9–harboring cells were infected with GFP-U6-sgGFP or GFP-U6-sgMafg1 and selected with hygromycin, and polyclonal populations were used for experiments. (b) TRE-Cas9–harboring mouse melanoma cell lines were infected with a GFP-U6-sgGFP reporter construct. Western blot showed that Dox treatment resulted in Cas9 (Flag) expression and a decrease in GFP levels. (c) TRE-Cas9–harboring M10M3 and M167M1 cells were infected with GFP-U6-sgGFP or GFP-U6-sgMafg1. Cells were then treated with Dox, and Flag-Cas9, GFP, and MAFG expressions were analyzed by western blot. Cas9 was expressed on Dox treatment, GFP was decreased in sgGFP-expressing cells, and MAFG was decreased in sgMafg1-expressing cells. (d) M10M3 and (e) M167M1 cells harboring TRE-Cas9 and sgGFP or sgMafg1 were plated at a low density, and colony-forming ability was examined, which is shown as percent surface area covered by colonies. (f) M10M3 and (g) M167M1 cells harboring TRE-Cas9 and sgGFP or sgMafg1 were plated in soft agar, and anchorage-independent growth was examined. Dox, doxycycline; sgGFP, sgRNA targeting GFP; sgMafg1, sgRNA targeting *Mafg*.

MAFG depletion impaired colony formation and anchorage-independent growth in BPP cells (M10M3) but had only modest effects in BCC cells (M167M1) (Figure 6d–g). This may suggest the possibility of the genotype-specific significance of *Mafg*, which warrants further investigation. Overall, the regulatory alleles enable inducible gene depletion by CRISPR/Cas9 and could prove useful for reversible expression of cDNA or short hairpin RNA constructs.

In summary, we generated 21 mouse melanoma cell lines harboring clinically relevant genetic drivers. Most of these cell lines form tumors when allografted into syngeneic recipients. In addition, these lines contain CHC and rTA3 alleles for the genomic insertion and regulation of transgenic constructs. The utility of these cell lines may be further assessed and improved, for instance, by optimizing CHC

targeting, by generating UV-irradiated derivatives, by isolating single-cell clones with high Cas9 activity, or by testing the sensitivity of additional lines to checkpoint inhibition. This cell line panel includes the first seven cell lines derived from melanomas driven by the LSL-*Nras*^{Q61R} allele (Burd et al., 2014), whereas previously reported *Nras*-mutant cell lines were derived from *Tyr::Nras*^{Q61K} melanomas (Dorard et al., 2017; Lindsay et al., 2011; Petit et al., 2019; Swoboda et al., 2021). Interestingly, melanomas in LSL-*Braf*^{V600E} and LSL-*Nras*^{Q61R} mice are almost uniformly amelanotic. This could be explained by the downregulation of *Mitf* (Figure 2a and b) in these tumors, which also results in the downregulation of transgenes under the control of the tyrosinase promoter such as Tyr-CreERT2 (Bok et al., 2020 and Figure 3a). Thus, our murine melanoma cell lines may

represent human melanomas having low MITF expression. It is possible that in melanomas driven by the *Tyr::Nras^{Q61K}* transgene, where mutant *Nras* is under the control of the tyrosinase promoter, the MITF-regulated gene program remains active to maintain the expression of mutant *Nras*. However, whether *Tyr::Nras^{Q61K}* tumors and cell lines model MITF-high human melanomas and whether these two *Nras* alleles model different subtypes of human melanoma remain to be investigated. With the establishment of the LSL-*Nras^{Q61R}* cell lines, comparative studies are now possible. Taken together, this panel of murine melanoma cell lines will further expand the resources available for investigating melanoma biology and therapies, and it will be made available to the melanoma research community.

MATERIALS AND METHODS

Mouse melanoma cell line generation

Melanoma cells were isolated from ESC-derived GEMMs and cell lines established as previously described (Bok et al., 2020). Briefly, tumor tissues were collected and washed in 70% ethanol for 10 seconds and rinsed in PBS. Diced tumor tissues were then digested in 1 mg/ml collagenase/dispase (catalog number 10269638001; Sigma-Aldrich, St. Louis, MO) for 20 minutes in a humidified incubator at 37 °C. Tissues were then washed with PBS and further digested in 0.25% Trypsin (catalog number VWRL0154-0100; VWR, Radnor, PA) for 30 minutes in the incubator. Cells were spun down and plated in RPMI containing 5% fetal bovine serum (FBS) and 1% penicillin/streptomycin. Cells isolated from *Braf^{V600E}*, *Pten^{FL/FL}* and *Nras^{Q61R}*; *Pten^{FL/FL}* tumors were expanded in vitro for several days, followed by subcutaneous injection into athymic nude mice (J:NU Stock number 007850; The Jackson Laboratory, Bar Harbor, ME) before the onset of in vitro growth arrest. Cell lines derived from allografted tumors were established similar to spontaneous ESC-derived GEMM melanomas.

Cell culture

Mouse melanoma cell lines and SW1 cell line (a gift from Eric Lau) were cultured in RPMI containing 5% FBS and 1% penicillin/streptomycin in a humidified incubator at 37 °C with 5% carbon dioxide. Melan-a was cultured in RPMI containing 10% FBS and 1% penicillin/streptomycin supplemented with 200 nM 12-O-Tetradecanoylphorbol-13-acetate (catalog number P8139; Sigma-Aldrich), 200 pM Cholera Toxin (catalog number C8052; Sigma-Aldrich) in a humidified incubator at 37 °C with 10% carbon dioxide.

Genomic DNA isolation and LSL-recombination genotyping PCR

Mouse melanoma cells were harvested by scraping. Cells were lysed in lysis buffer (5% 2 M Tris, pH 7.5, 2% 5 M sodium chloride, 1% 0.5M EDTA, 2% of 10% SDS, and 90% double distilled water) containing proteinase K overnight at 56 °C. DNA was precipitated by adding 100% ethanol, and the pellet was washed with 70% ethanol. The DNA pellet was then air dried and resuspended in DNase/RNase-free water. The PCR primers used for LSL-recombination genotyping of LSL-*Braf^{V600E}* were as follows: 5'-CAAA-CACCTGAGTCTATGGG-3' (common forward) for LSL-*Braf^{V600E}* and 5'-CCGGGATGCAGAAATTGATG-3' (reverse) for LSL and 5'-GATT-CACATGGGACCTGAAC-3' (reverse) for wild-type. The primers for LSL-*Nras^{Q61R}* were reported previously (Burd et al., 2014).

RNA isolation and *Nras* exon amplification

Mouse melanoma cells were lysed with QIAzol lysis reagent (catalog number 79306; Qiagen, Hilden, Germany), and RNA was isolated as per the manufacturer's instructions. cDNA synthesis was performed using 500 ng RNA and the PrimeScript RT master mix (catalog number RR036A; Takara Bio, Kusatsu, Japan). PCR was performed using the Go-Taq Green master mix (catalog number M7123; Promega, Madison, WI) with the following primers to amplify *Nras* exons 1–3: 5'-GACTGAGTACAACTGGTGG-3' (forward) for *Nras*-ex1 and 5'-GCTTGCTTTGTGTCAACTGTC-3' (reverse) for *Nras*-ex3-R. The PCR products were separated by gel electrophoresis and purified using the E.Z.N.A. Gel extraction kit (catalog number 101318-972; Omega Bio-Tek, Norcross, GA). Sanger sequencing was performed by Eton Bioscience (San Diego, CA).

Allograft experiments

All animal experiments were conducted in accordance with an Institutional Animal Care and Use Committee protocol (R-1S00005420) approved by the University of South Florida (Tampa, FL). Mouse melanoma cells were injected into C57BL/6J (stock number 000664; The Jackson Laboratory) or NSG gamma (stock number 005557; The Jackson Laboratory) bred in house. Tumors were measured using calipers, and volume was calculated using the formula (width² × length) / 2. Mice were fed chow containing 200 mg/kg Dox purchased from Envigo (Indianapolis, IN).

Anti-PD-1 and IgG treatment

C57BL/6J mice were purchased from the Charles River National Cancer Institute facility. Mice were aged 10 weeks at the time of tumor implantation. Melanoma cell lines were intradermally injected onto the backs of mice. Mice were given a total of five injections of 200 µg/ml IgG2AK (#400566; BioLegend, San Diego, CA) or anti-PD-1 (#114115, clone RMP1-14; BioLegend) commencing on the development of a palpable tumor. On the basis of weight loss, no toxicity was observed.

CHC targeting of mouse melanoma cell lines by RMCE

Mouse melanoma cell lines were targeted as previously described (Bok et al., 2020). Briefly, cells were cotransfected with 2 µg pCAGGS-FLPe plasmid and 4 µg COL1A1-EF1α-GFP targeting vector at a 1:2 ratio using FuGENE HD Transfection Reagent (catalog number E2311; Promega) according to the manufacturer's instructions, followed by selection in 50 µg/ml hygromycin. GFP-positive cells were assessed after 3 weeks.

Plasmids and virus transduction

High-fidelity, codon-optimized Cas9 was cloned from pLenti-HF1RA-PGK-Puro (Zafra et al., 2018), a gift from Lukas Dow (plasmid number 110860; Addgene, Watertown, MA), by replacing GFP in pLenti-TRE-GFP-Blast by In-Fusion cloning (catalog number 638911; Takara Bio). Primers used for cloning were 5'-AGCTTGCGTTGGATCCGCCACCATGGATTACAAAG-3' (forward) Cas9 and 5'-GAGGTTGATTGTGCGACTTATTTCTTTTCTTAGCTTGACCAGCTTTCT-3' (reverse) for Cas9.

The generation of pLenti-TRE-GFP-Blast was previously described (Bok et al., 2020). A sgRNA targeting murine *Mafg* was cloned by oligocloning (sense 5'-CACCGTTATGACGACCCCAATAA-3', antisense 5'-AACTTATTGGGGTTCGTCATAAC-3') into lentiCRISPRv2 (Sanjana et al., 2014), a gift from Feng Zhang (plasmid number 52961, Addgene; provided by Tyler Jacks). sgRNA cutting efficiency of *Mafg* was validated by western blot of mouse embryonic fibroblasts infected with sgRNA_lentiCRISPRv2. The U6-sgRNA cassette

was then cloned by InFusion cloning (*U6* 5'-CAACCCGAGGG-GACCCGAGGGCCTATT-3' [forward] and *U6* 5'-CGGGCCTGTCGGGTCGCTAGCGAATTCAAAAAAGCACCG-3' [reverse]) in the KflI restriction site of pLenti-GFP-Hygro. The *U6*-sgGFP-gRNA scaffold cassette from pXPR_011 (Doench et al., 2014), a gift from John Doench and David Root (plasmid number 59702, Addgene; provided by Gina DeNicola), was cloned into pLenti-GFP-Hygro using the same approach. Lentivirus production and transduction were performed as previously described (Bok et al., 2020). M10M7 cells were infected with Ad5CMVCre adenovirus purchased from the University of Iowa Viral Vector Core (<https://vector-core.medicine.uiowa.edu/>).

Immunoblotting

Immunoblotting was performed as previously described (Bok et al., 2020). Antibodies against FLAG (1:1,000, catalog number 14793S; Cell Signaling Technology, Danvers, MA), GFP (1:2,000, catalog number 2956S; Cell Signaling Technology), MAFG (1:1,000, catalog number ab154318; Abcam, Cambridge, United Kingdom), p16INK4a (1:2,000, catalog number ab211542; Abcam), p19ARF (1:1,000, catalog number ab80; Abcam), p53 (1:1,000, catalog number 3036-100; BioVision, Milpitas, CA), phosphorylated AKT S473 (1:2,000, catalog number 9188S; Cell Signaling Technology), phosphorylated AKT T308 (1:500, catalog number 13038T; Cell Signaling Technology), AKT (1:5,000, catalog number 4691T; Cell Signaling Technology), phosphorylated ERK T202/Y204 (1:1,000, catalog number 9101S; Cell Signaling Technology), ERK (1:1,000, catalog number 4695S; Cell Signaling Technology), S100B (1:1,000, catalog number ab52942; Abcam), MART1 (1:1,000, catalog number SAB4500949-100UG; Sigma-Aldrich), Cre (1:1,000, catalog number ab190177; Abcam), MITF (1:1,000, catalog number 12590S; Cell Signaling Technology), and β -actin (1:10,000, catalog number AM4302; Thermo Fisher Scientific, Waltham, MA) were used.

Colony formation assay

Cells were treated with 0.5 μ g/ml Dox (catalog number D9891-1G; Sigma-Aldrich) for 3 days, followed by culture in Dox-free media for 2–3 days to inactivate Cas9 expression. A total of 500 cells were seeded in six-well plates in triplicates and incubated for 8 days. Cells were fixed in cold 4% paraformaldehyde (catalog number 101176-014; VWR) and stained with 0.5% crystal violet (catalog number 97061-850; VWR). Percent area of crystal violet staining was quantified using ImageJ (National Institutes of Health, Bethesda, MD).

Soft agar assay

For the bottom layer, 0.8% SeaPlaque agarose (catalog number 50101, Lonza, Basel, Switzerland) in RPMI containing 10% FBS and 1% penicillin/streptomycin was plated onto six-well plates and solidified at room temperature. For the upper layer, 0.4% agarose in RPMI containing 10% FBS and 1% penicillin/streptomycin mixed with 3,000–5,000 cells were plated and overlaid with 1 ml RPMI with 5% FBS and 1% penicillin/streptomycin once solidified. After 14 days, plates were stained with 0.001% crystal violet overnight at 4 °C. The number of colonies was quantified using ImageJ.

Statistical analysis

Statistical analysis was performed using GraphPad Prism software (GraphPad Software, San Diego, CA) and Microsoft Excel (Microsoft, Redmond, WA). Data were analyzed with unpaired two-tailed *t*-test, and *P* < 0.05 was considered statistically significant.

Data availability statement

No datasets were generated or analyzed during this study.

ORCIDiS

Ilah Bok: <http://orcid.org/0000-0001-8958-5161>
 Ariana Angarita: <http://orcid.org/0000-0001-6795-4640>
 Stephen M. Douglass: <http://orcid.org/0000-0003-1562-2235>
 Ashani T. Weeraratna: <http://orcid.org/0000-0003-0448-6952>
 Florian A. Karreth: <http://orcid.org/0000-0002-2350-9809>

AUTHOR CONTRIBUTIONS

Conceptualization: FAK; Investigation: IB, AA, SMD, FAK; Methodology: IB, FAK; Supervision: FAK; Writing - Original Draft Preparation: IB, FAK; Writing - Review and Editing: IB, AA, SMD, ATW, FAK

ACKNOWLEDGMENTS

We thank the members of the Karreth laboratory for their critical reading of the manuscript. This work was supported by grants to FAK from the National Institutes of Health/National Cancer Institute (R03 CA227349 and R01 CA259046) and the Melanoma Research Alliance (Melanoma Research Alliance Young Investigator Award, <https://doi.org/10.48050/pc.gr.75702>) and to ATW from the National Institutes of Health/National Cancer Institute (R01 CA207935 and P01 CA114046). This work was also supported by the Gene Targeting Core and Biostatistics and Bioinformatics Core, which are funded in part by Moffitt's Cancer Center Support Grant (P30-CA076292).

CONFLICT OF INTEREST

ATW is on the Board of Directors for ReGAIN therapeutics. The remaining authors state no conflict of interest.

REFERENCES

- Bok I, Vera O, Xu X, Jasani N, Nakamura K, Reff J, et al. A versatile ES cell-based melanoma mouse modeling platform. *Cancer Res* 2020;80:912–21.
- Burd CE, Liu W, Huynh MV, Waqas MA, Gillahan JE, Clark KS, et al. Mutation-specific RAS oncogenicity explains NRAS codon 61 selection in melanoma. *Cancer Discov* 2014;4:1418–29.
- Doench JG, Hartenian E, Graham DB, Tothova Z, Hegde M, Smith I, et al. Rational design of highly active sgRNAs for CRISPR-Cas9-mediated gene inactivation. *Nat Biotechnol* 2014;32:1262–7.
- Dorard C, Estrada C, Barbotin C, Larcher M, Garancher A, Leloup J, et al. RAF proteins exert both specific and compensatory functions during tumour progression of NRAS-driven melanoma. *Nat Commun* 2017;8:15262.
- Hooijkaas AI, Gadiot J, van der Valk M, Mooi WJ, Blank CU. Targeting BRAFV600E in an inducible murine model of melanoma. *Am J Pathol* 2012;181:785–94.
- Jeck WR, Parker J, Carson CC, Shields JM, Sambade MJ, Peters EC, et al. Targeted next generation sequencing identifies clinically actionable mutations in patients with melanoma. *Pigment Cell Melanoma Res* 2014;27:653–63.
- Jenkins MH, Steinberg SM, Alexander MP, Fisher JL, Ernstoff MS, Turk MJ, et al. Multiple murine BRAF(V600E) melanoma cell lines with sensitivity to PLX4032. *Pigment Cell Melanoma Res* 2014;27:495–501.
- Koya RC, Mok S, Otte N, Blacketer KJ, Comin-Anduix B, Tumei PC, et al. BRAF inhibitor vemurafenib improves the antitumor activity of adoptive cell immunotherapy. *Cancer Res* 2012;72:3928–37.
- Lindsay CR, Lawn S, Campbell AD, Faller WJ, Rambow F, Mort RL, et al. P-Rex1 is required for efficient melanoblast migration and melanoma metastasis. *Nat Commun* 2011;2:555.
- Meeth K, Wang JX, Micevic G, Damsky W, Bosenberg MW. The YUMM lines: a series of congenic mouse melanoma cell lines with defined genetic alterations. *Pigment Cell Melanoma Res* 2016;29:590–7.
- Pérez-Guijarro E, Yang HH, Araya RE, El Meskini R, Michael HT, Vodnala SK, et al. Multimodel preclinical platform predicts clinical response of melanoma to immunotherapy [published correction appears in *Nat Med* 2021;27:355]. *Nat Med* 2020;26:781–91.
- Petit V, Raymond J, Alberti C, Pouteaux M, Gallagher SJ, Nguyen MQ, et al. C57BL/6 congenic mouse NRAS^{Q61K} melanoma cell lines are highly sensitive to the combination of Mek and Akt inhibitors in vitro and in vivo. *Pigment Cell Melanoma Res* 2019;32:829–41.
- Sanjana NE, Shalem O, Zhang F. Improved vectors and genome-wide libraries for CRISPR screening. *Nat Methods* 2014;11:783–4.

I Bok et al.

ESC-GEMM-Derived Murine Melanoma Cell Lines

Swoboda A, Soukup R, Eckel O, Kinslechner K, Wingelhofer B, Schörghofer D, et al. STAT3 promotes melanoma metastasis by CEBP-induced repression of the MITF pathway. *Oncogene* 2021;40:1091–105.

Vera O, Bok I, Jasani N, Nakamura K, Xu X, Mecozzi N, et al. A MAPK/miR-29 axis suppresses melanoma by targeting MAFG and MYBL2. *Cancers (Basel)* 2021;13:1408.

Wang J, Perry CJ, Meeth K, Thakral D, Damsky W, Micevic G, et al. UV-induced somatic mutations elicit a functional T cell response in the YUMMER1.7 mouse melanoma model. *Pigment Cell Melanoma Res* 2017;30:428–35.

Zafra MP, Schatoff EM, Katti A, Foronda M, Breinig M, Schweitzer AY, et al. Optimized base editors enable efficient editing in cells, organoids and mice. *Nat Biotechnol* 2018;36:888–93.



This work is licensed under a Creative Commons Attribution-NonCommercial-NoDerivatives 4.0 International License. To view a copy of this license, visit <http://creativecommons.org/licenses/by-nc-nd/4.0/>